Nanopore Unitary Permeability Measured by Electrochemical and Optical Single Transporter Recording

Roland Hemmler,* Guido Böse,*† Richard Wagner,‡ and Reiner Peters*†
*Institut für Medizinische Physik und Biophysik, Universität Münster, Münster, Germany; †Center of Nanotechnology, Münster, Germany; and ‡Fachbereich Biologie, Universität Osnabrück, Osnabrück, Germany

ABSTRACT For the analysis of membrane transport processes two single molecule methods are available that differ profoundly in data acquisition principle, achievable information, and application range: the widely employed electrical single channel recording and the more recently established optical single transporter recording. In this study dense arrays of microscopic horizontal bilayer membranes between 0.8 μm and 50 μm in diameter were created in transparent foils containing either microholes or microcavities. Prototypic protein nanopores were formed in bilayer membranes by addition of *Staphylococcus aureus* α-hemolysin (α-HL). Microhole arrays were used to monitor the formation of bilayer membranes and single α-HL pores by confocal microscopy and electrical recording. Microcavity arrays were used to characterize the formation of bilayer membranes and the flux of fluorescent substrates and inorganic ions through single transporters by confocal microscopy. Thus, the unitary permeability of the α-HL pore was determined for calcein and Ca^{2+} ions. The study paves the way for an amalgamation of electrical and optical single transporter recording. Electro-optical single transporter recording could provide so far unresolved kinetic data of a large number of cellular transporters, leading to an extension of the nanopore sensor approach to the single molecule analysis of peptide transport by translocases.

INTRODUCTION

The bilayer method for electrical single channel recording has been used to characterize a large number of native and recombinant ion channels (Favre et al., 2004). Furthermore the method has been employed in a ''footprint''like version (Simon et al., 1989) using the flux of ions as indicator for the existence, properties, and status of aqueous transmembrane channels. Thus, the early hypothesis (Blobel and Dobberstein, 1975) that the translocation of newly synthetized proteins through the membrane of the endoplasmic reticulum (ER) involves an aqueous transmembrane channel was eventually verified (Simon et al., 1989) by fusing ER vesicles with bilayer membranes and observing single channel currents in dependence of protein synthesis conditions. By the same approach protein conducting channels (PCC) have been identified as central elements of other translocases, especially those of mitochondria (Hill et al., 1998; Truscott et al., 2001; Kovermann et al., 2002; Rehling et al., 2003) and chloroplasts (Heins et al., 2002).

Recently, the ''footprint'' approach has found biotechnological applications. Using the stable nongated nanopore (Song et al., 1996) formed by *Staphylococcus aureus* α-hemolysin (α-HL) the blockade of the single channel current caused by substrate molecules in transient was used to obtain information about the identity, concentration, and primary structure of the substrate (Kasianowicz et al., 1996; Bayley and Cremer, 2001). Importantly, the base sequence of polynucleotides has been determined at very high speed (Akeson et al., 1999; Meller et al., 2000) although a true de novo DNA sequencing has yet to be achieved.

To measure the translocation through PCCs not only of ions but also macromolecules we have developed Optical Single Transporter Recording (OSTR) (Peters et al., 1990, 2003; Tschödrich-Rotter et al., 1996; Tschödrich-Rotter and Peters, 1998; Siebrasse and Peters, 2002; Kiskin et al., 2003). In OSTR a small chamber is employed having a micro- or nanostructured bottom referred to as the OSTR chip. This is a flat transparent foil containing dense arrays of small cylindrical cavities, the test compartments (TC). Measurements are done by firmly attaching cell membranes to OSTR chips, adding a fluorescent transport substrate to the chamber, and monitoring substrate transport across TC-spanning membrane patches into TCs by confocal fluorescence microscopy. Time resolution can be improved by employing photobleaching or photoactivation for initiating transport (Siebrasse and Peters, 2002). The transport of nonfluorescent substrates such as inorganic ions can be measured if substrate-specific fluorescent indicators are available (Tschödrich-Rotter et al., 1996). The TC diameter can be varied within wide limits (~0.1 μm–100 μm) so that TC-spanning membrane patches may contain single transporters or transporter populations of various sizes. OSTR is able to monitor, at single transporter resolution, the very small transport rates characteristic of carriers and pumps (10^0–10^3 substrate molecules/s). Multiplexing of transport substrates and massive parallel measurements are other features.

So far, OSTR has been mainly applied to the transport of proteins through the nuclear pore complex. In this study,

Submitted December 21, 2004, and accepted for publication February 18, 2005.

Address reprint requests to Dr. Reiner Peters, Institut für Medizinische Physik und Biophysik, Robert-Koch-Strasse 31, 48149 Münster, Germany. Tel.: 49-251-8356933; Fax: 49-251-8355121; E-mail: petersr@uni-muenster.de.

0006-3495/05/06/4000/08 $2.00

doi: 10.1529/biophysj.104.058255

OSTR was extended to a prototypic biological nanopore reconstituted in artificial bilayers. This paves the way for analyzing the variety of cellular nanochannels which can be reconstituted in artificial bilayers and also for making use of those nanochannels in nanotechnological applications.

MATERIALS AND METHODS

Materials

Chemicals, organic solvents, S-IV soy bean lipid, and α-HL were purchased from Sigma-Aldrich (St. Louis, MO). Calcein, calcium green-5N, and $DiOC_{18}$ were from Molecular Probes (Eugene, OR). Laser-structured arrays containing microcavities or single microholes were produced by Bartels Mikrotechnik (Dortmund, Germany). Polycarbonate track-etched membrane filters were obtained from Whatman International (Maidstone, England).

Preparation of bilayer membranes and creation of α-hemolysin pores

S-IV-lipid was kept at −20°C in chloroform/methanol (1:1) at 0.1 mg/ml. After vacuum evaporation of 65 μl of the stock solution the lipid was resuspended in 85 μl *n*-decane. Planar lipid bilayers were created using a modified painting technique (Mueller et al., 1962) as described in Results. For the visualization of bilayer membranes 3.5 μl of $DiOC_{18}(3)$ (1 mg/ml in MeOH) were added to the S-IV-lipid before evaporation to yield a dye/lipid molar ratio of ~1:2,000. To create transmembrane pores a few microliters of α-HL stock solution (0.5 mg/ml) was injected into the *cis*-compartment above the filter or TC array spanning the hole in the partition.

Confocal microscopy and electrical measurements

A confocal laser scanning system based on an upright microscope (Leica, Heidelberg, Germany) was complemented with a headstage preamplifier (CV-5-1GU, Axon Instruments, Union City, CA) and $Ag^+/AgCl_2$ electrodes. Currents were further amplified by a GeneClamp 500B amplifier, digitized using a Digidata 1322A (both Axon Instruments) and stored on a PC. For confocal imaging the 488 nm line of an Ar-Kr laser was employed together with a HCX APO 63 × 0.90 W objective (Leica Camera AG, Solms, Germany). The optical resolution was determined as described previously (Kubitscheck and Peters, 1998) to be ~400 nm (full width half-maximum, FWHM) in the optical plane and ~700 nm (FWHM) in direction of the optical axis.

RESULTS

In this study, an electro-optical single transporter recording chamber with two compartments was employed (Fig. 1). The horizontal partition had a hole of ~2 mm diameter which was spanned by a thin foil (''chip'') containing arrays of microholes or TCs. Chips were created from 100 μm thick polycarbonate foils by laser drilling (Peters, 2003). In some experiments, ~10 μm thick polycarbonate track-etched membrane filters were employed instead of laser structured chips. Three sizes of microholes/TCs were employed with diameters of 30–70 μm, 5.0 μm, or 0.8 μm diameter, respectively. In each experimental series at first microhole chips were used to monitor the formation of bilayer membranes and the creation of α-HL pores by simultaneous confocal microscopy and electrical recording. Subsequently, TC chips were employed to visualize the formation of bilayer membranes and to measure the flux of fluorescent tracers through α-HL pores by confocal microscopy.

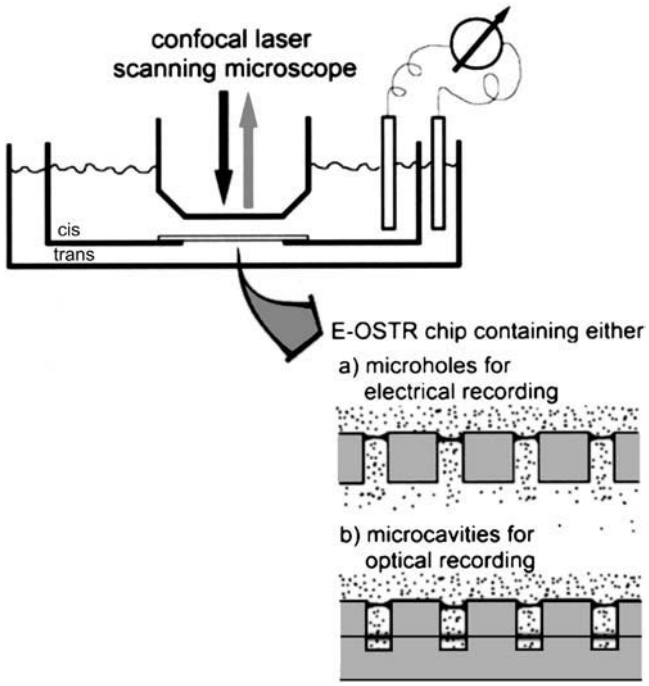

FIGURE 1 Scheme of the experimental setup used for the electrical and optical recording of single nanopores in bilayer microarrays.

Proof of principle experiments

Chips containing a single hole of 30–70 μm diameter were used. The chamber was filled with buffer (250 mM KCl, 10 mM Mops/TRIS, pH 7.0) and a droplet of ~0.1 μl of soy bean lipid, dissolved in *n*-decane and doped with the fluorescent lipid analog $DiOC_{18}$, deposited close to the microhole. The lipid was spread across the hole using the tip of a thin plastic rod and the formation of bilayer membranes visualized by confocal scans. The typical appearance of a bilayer membrane is shown in Fig. 2 *A*. In horizontal (*xy*) scans (Fig. 2 *A*, *left*) the lipid annulus was evident as a brightly fluorescent ring whereas the central bilayer area remained virtually invisible. The bilayer area was easily visualized, however, by more sensitive equipment (Kubitscheck et al., 2000) involving a focused laser beam and a cooled CCD camera (data not shown). In vertical (*xz*) scans (Fig. 2 *A*, *right*) the bilayer area became directly visible as a faintly fluorescent line. The thickness of the lipid annulus surrounding the bilayer area varied from one experiment to another yielding bilayers of various sizes. The area of individual bilayers ($n = 15$) was determined from confocal scans and correlated with their electrical capacitance. A linear relationship with a slope of 0.14 $\mu F/cm^2$ was found, as normal for bilayer membranes

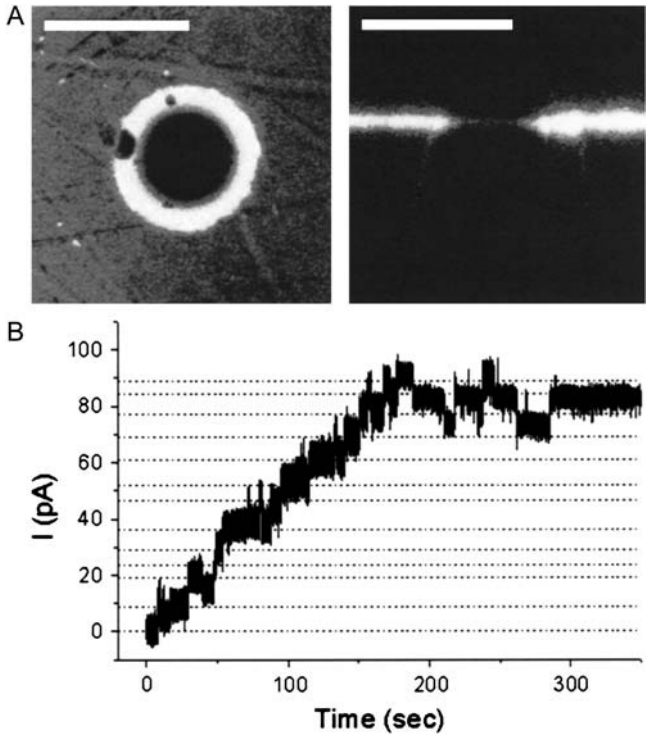

FIGURE 2 Creation of bilayer membranes spanning 50 μm holes and electrical recording of nanopore formation in those bilayer membranes. (*A*) Horizontal (*left*) and vertical (*right*) confocal scans of a bilayer membrane doped with a fluorescent lipid analog. The lipid annulus displays a strong, the bilayer region a dim fluorescence. Scale bars, 50 μm. (*B*) Formation of α-HL pores in the bilayer membrane as indicated by current steps (mean step size 7.2 pA at 30 mV, 250 mM KCl).

(Micelli et al., 2002). Upon injection of a few microliters of an α-hemolysin solution into the *cis*-compartment (cf. Fig. 1 for nomenclature, final α-HL concentration ~100 nM) a stepwise increase in electrical current was observed (Fig. 2 *B*). After a few minutes, the current assumed a constant value, probably because all α-HL was bound to the excess of lipid in the *cis*-compartment. On average the current increase consisted of 10–20 steps with a mean step size of 7.2 pA at 30 mV, 250 mM KCl, as characteristic for the α-HL pore (Krasilnikov et al., 1981) (cf. Discussion).

In separate experiments chips containing TCs of 70 μm diameter and 50 μm depth (Kiskin et al., 2003) were employed. When lipid was applied to the chip and spread across a TC, bilayer membranes formed as directly visualized by confocal scans (Fig. 3 *A*). After bilayer membrane formation the small hydrophilic fluorescent probe calcein (final concentration 1 μM) and α-HL (final concentration 100 nM) were injected into the *cis*-compartment one after the other and the TC was imaged by a series of vertical scans (Fig. 3 *B*). After a slight lag resulting from time needed for diffusion and insertion of α-HL into the bilayer, it was found that calcein entered slowly into the TC (Fig. 3 *C*, *solid symbols* and *solid line*). If α-HL was omitted calcein was perfectly excluded from TCs (Fig. 3 *C*, *open symbols* and *dotted line*).

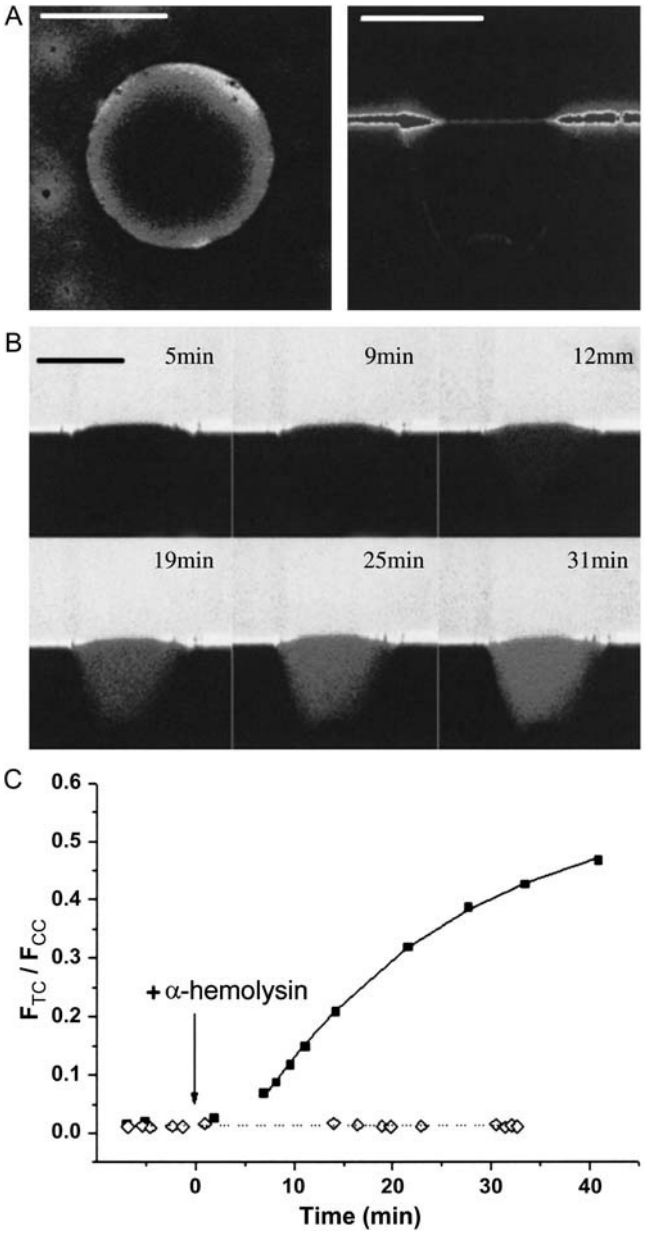

FIGURE 3 Creation of bilayer membranes spanning test compartments of 70 μm diameter and optical recording of transport through nanopores in those bilayer membranes. (*A*) Horizontal (*left*) and vertical (*right*) confocal scans of a bilayer membrane doped with a fluorescent lipid analog. Scale bars, 50 μm. (*B*) Transport of the small hydrophilic fluorescent tracer calcein through a bilayer membrane containing α-HL pores. Scale bar, 50 μm. (*C*) Transport kinetics obtained by normalizing the fluorescence in the test compartment (F_{TC}) by the fluorescence in the *cis*-compartment (F_{CC}) and plotting versus time. The lag between addition of α-HL and the onset of calcein transport is due to the time needed for α-HL molecules to diffuse to the TC array, to insert into bilayer membranes and to form pores by oligomerization. Full symbols: experimental data derived from *B*. Open symbols, control experiment of bilayer membranes without α-HL pores.

The experiments showed that it is possible to create TC-spanning bilayers, to insert α-HL pores into those bilayers and to optically monitor the flux of a fluorescent substrate through the α-HL pores. To derive unitary permeability coefficients, however, a slightly different method is required.

Unitary permeability of the α-hemolysin pore

In a second experimental series track-etched membrane filters with pores of 5.0 μm diameter were employed as microhole chips spanning a hole of ~2 mm diameter. Experimental procedures were essentially as described for single 30–70 μm holes. However, care was taken to spread the lipid all over the available filter area to avoid leakage through open pores. Confocal scans (Fig. 4 *A*) suggested that microscopic bilayer membranes formed easily across filter pores. Upon addition of α-HL (final concentration 100 nM) after bilayer formation, the transmembrane current increased stepwise (Fig. 4 *B*) with a mean step size (31 pA at 1M KCl, 30 mV) characteristic for the α-HL pore. Thus, the electrical recording confirmed that bilayer membranes had been formed and α-HL pores were inserted. The total number of α-HL pores created per experiment was determined by counting voltage steps to be ~100 on average. The number of filter pores in the filter piece forming the bottom of the chamber was derived from the average filter pore density (4×10^5 cm^{-2}) and the area of the chamber bottom (~0.03 cm^2) to be ~12,000. Thus, the average number of α-HL pores/filter pore was ~0.01. However, the homogeneity of bilayer formation and α-HL pore insertion could not be assessed by electrical measurements. Optical transport measurements described below suggested that bilayer membranes did not form on all filter pores but that a fraction of filter pores remained occluded by lipid droplets.

To further investigate the possibilities for creating arrays of miniature bilayer membranes, track-etched filters with pores of 0.8 μm diameter were employed. In contrast to pores of 5 μm or 50 μm diameter no direct visualization of bilayer membranes was possible in the case of 0.8 μm filter pores. At a lateral optical resolution of 0.4 μm FWHM (see Methods) the bright fluorescence of the lipid annuli outshone the very weak fluorescence of the bilayer membranes. However, after α-HL addition the transmembrane current increased stepwise (Fig. 4 *C*) with a mean step size of 34.5 pA (1M KCl, 30 mV).

Optical transport measurements on many bilayer membranes were performed in parallel using regular laser-structured arrays (Fig. 5, *A* and *B*). The conelike TCs had an entrance of ~5 μm diameter, a depth of ~7 μm, and a pitch of 10 μm determined by laser scanning microscopy of free fluorophore in solution, resulting in a calculated volume of ~50 fl. Experimental procedures were essentially as described for 5.0 μm holes. Confocal scans (Fig. 5 *A*) suggested that the spreading of lipid created three fractions of TCs, one completely void of lipid, a second covered by bilayer membranes, and a third occluded by lipid droplets. The magnitude of the TC fractions could be varied to a certain extent by adjusting the amount of lipid and its spreading. In particular, the first fraction could be completely eliminated by very carefully spreading the lipid over the whole available array.

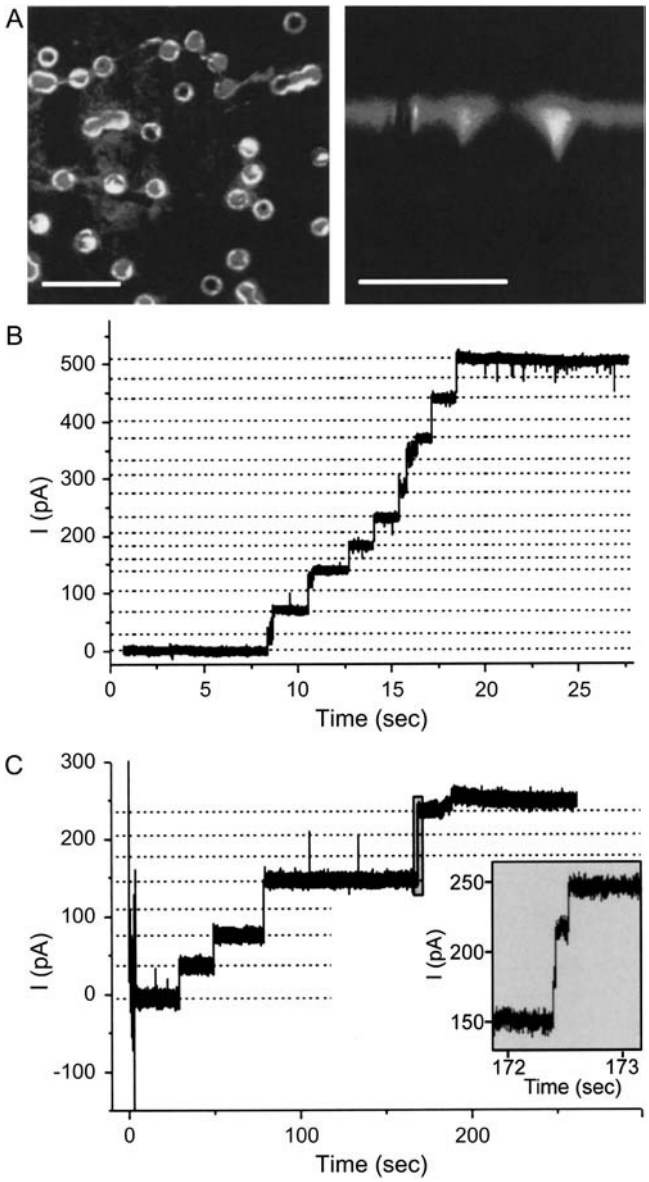

FIGURE 4 Formation of bilayer membranes spanning pores of track-etched membrane filters and electrical recording of nanopore formation in those bilayer membranes. (*A*) Horizontal (*left*) and vertical (*right*) confocal scans of bilayer membranes spanning filter pores of 5 m diameter. Most of the filter pores are spanned by bilayer membranes. Occasionally, pores occluded by lipid droplets are seen. Scale bars, 20 μm (*left*) and 10 μm (*right*). (*B*) Formation of α-HL pores in 5 μm bilayer membranes as indicated by current steps (mean step size 34.5 pA at 30 mV, 1 M KCl). (*C*) Formation of α-HL pores in 0.8 μm bilayer membranes as indicated by current steps. (*Inset*) Resolution of a large step into three unitary steps.

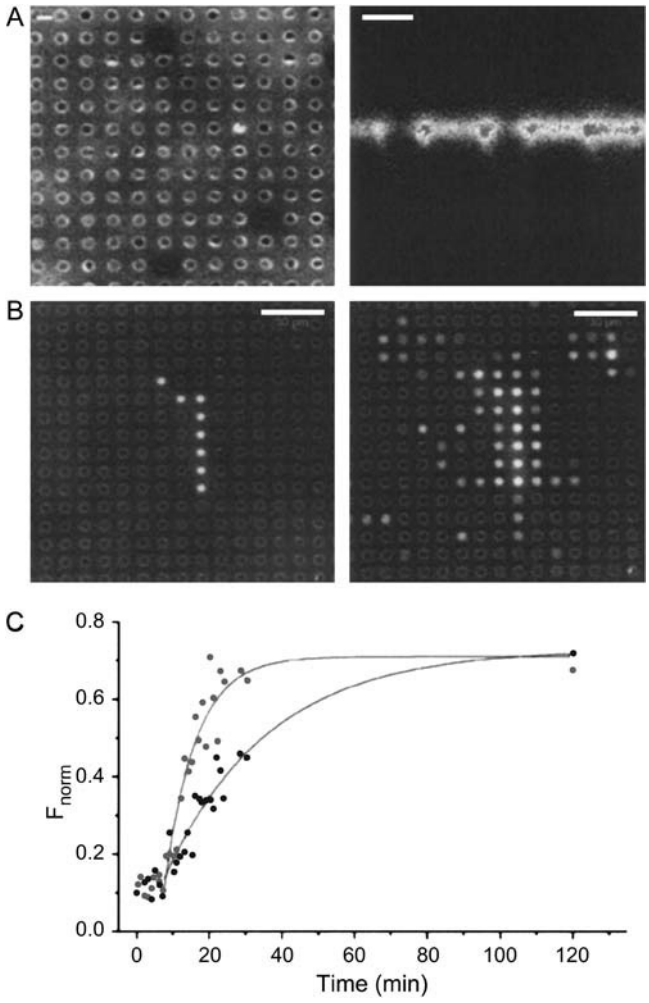

FIGURE 5 Creation of bilayer membranes spanning test compartments of 5 μm diameter and optical recording of transport through nanopores in those bilayer membranes. (*A*) Horizontal (*left*) and vertical (*right*) confocal scans of bilayer membranes. Scale bars, 5 μm. (*B*) Transport of calcein through bilayer membranes containing α-HL pores. (*Left*) In horizontal sections with the focal plane set to cut through the test compartments ~3–5 μm below the surface of the chip test, compartments lacking bilayer membranes are seen to be filled with calcein. (*Right*) Shortly after addition of α-HL to the *cis*-chamber, calcein appears in those test compartments covered by a bilayer membrane and having acquired one or a few α-HL pores. (*C*) Normalized fluorescence of two of the test compartments shown in (*B*). Normalization excludes fluctuations of image intensities caused by variations of z position or laser intensities.

After bilayer formation calcein was added to the *cis*-compartment. The specimen was positioned in z direction such that the optical section passed through the TC array ~3–5 μm below its surface. An area of the chip was chosen (Fig. 5 *B*, *left*) containing some TCs which had been filled immediately by calcein and were brightly fluorescent. Then, α-HL was added to the *cis*-compartment and transport recorded by a series of confocal scans. It was found (Fig. 5 *B*, *right*) that fluorescence increased with time in many but not all TCs. In TCs responding to the addition of α-HL the fluorescence increased steadily to reach within several minutes the level of those TCs that had been fluorescent before α-HL addition. Thus, three TC fractions were discriminated, here referred to as *a*, *b*, and *c*. For obvious reasons we assume that fraction *a*, showing a time- and α-HL-independent fluorescence, is composed of TCs void of lipid. Fraction *b*, responding to α-HL addition by a time-dependent fluorescence increase, is thought to be constituted of TCs covered by bilayer membranes containing one or more α-HL pores. Fraction *c*, remaining nonfluorescent independently of α-HL addition, may be constituted of TCs occluded by lipid droplets or spanned by bilayer membranes void of α-HL pores. Transport of calcein through α-HL pores was quantitated by deriving the fluorescence intensity for all type *a* and type *b* TCs of a series individually. For that purpose the image evaluation program described previously (Kiskin et al., 2003) was used. The program automatically localizes TCs in an image stack, determines the fluorescence intensities of circular areas slightly smaller than the TC cross section and corrects that fluorescence for background fluorescence measured in areas surrounding TCs. In these experiments, the fluorescence intensities of type-*a* TCs of a given image stack was averaged and the fluorescence of an individual type-*b* TC of the same stack was normalized by the average of type a TCs. Finally, the normalized fluorescence of type-*b* TCs was plotted versus time, as illustrated in Fig. 5 *C*.

For further analysis (Peters, 2003) the normalized fluorescence of single type-*b* TCs was fitted by mono-exponentials of the form $1-\exp(-kt)$. The rate constant k was determined for a substantial population of TCs at constant experimental conditions and the frequency of k in that population plotted versus k (Fig. 6 *A*). The histogram is seen to split up into distinct peaks distributed equidistantly on the k axis which is indicative of bilayer subpopulations carrying 1, 2, 3,... transporters. Such subpopulations arise when the distribution of transporters among bilayer membranes is random although the mean number of transporters per patch is small, conditions met by present experimental conditions. Thus, the largest peak in Fig. 6 *A* with $k = 0.03\ \text{min}^{-1}$ can be unambiguously attributed to bilayer membranes containing a single α-HL pore. The unitary permeability P_1 is given (Peters, 2003) by

$$P_1 = k_1 \times V_{\text{TC}}, \tag{1}$$

where V_{TC} is the TC volume. With $V_{\text{TC}} = 50$ fl and $k_1 = 0.03\ \text{min}^{-1}$, the unitary permeability of the α-HL pore for calcein becomes $P_1 = 2.5\ 10^{-2}\ \mu\text{m}^3\text{s}^{-1}$. The flux Φ (molecules/s/transporter) is related to the unitary permeability P_1 by

$$\Phi = P_1 \times N_{\text{A}} \times \Delta C, \tag{2}$$

where N_{A} is Avogadro's number and ΔC is the transmembrane concentration difference. Thus, the flux of calcein through α-HL pores is 15 molecules/s/pore at a concentration difference of 1 μM.

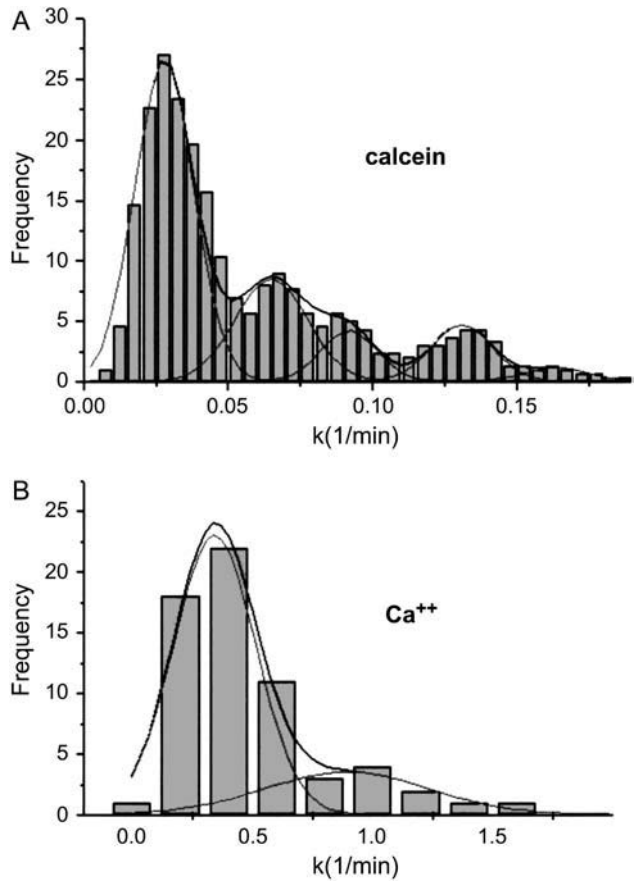

FIGURE 6 Unitary permeability of the α-HL pore for calcein and Ca^{2+}. Arrays of 5 μm diameter bilayer membranes containing <1 α-HL pore on average were used to measure the permeation of calcein or Ca^{2+} into test compartments. Plots of the frequency of the transport rate constant k versus k display distinct peaks representing bilayer membranes with 1, 2, 3, ... α-HL pores. For calcein and Ca^{2+}, the unitary rate constant k_1 (largest peak) was found to be $\sim$0.03 min^{-1} (*A*) and $\sim$0.35 min^{-1} (*B*), respectively. The histogram in *A* was derived from 238 k values obtained in 14 experiments, that in (*B*) from 63 k values obtained in nine experiments.

The unitary permeability of the α-HL pore for Ca^{2+} ions was determined (Fig. 6 *B*) by forming TC-spanning bilayer in a Ca^{2+}-free buffer containing the fluorescent Ca^{2+} indicator Oregon Green 5N at 1 μM. After bilayer membrane formation α-HL and Ca^{2+} (final concentration 1 mM) were sequentially added to the *cis*-compartment. Flux measurements were performed and data analyzed as in the case of calcein experiments yielding (Fig. 6 *B*) $k_1 = 0.35$ min^{-1} and $P_1 = 0.29$ $\mu m^3 s^{-1}$, which is similar to transport rates determined for the aerolysin pore (Tschödrich-Rotter et al., 1996). The flux of Ca^{2+}, according to Eq. 2, amounts to 175 ions/s/pore at a concentration difference of 1 μM.

DISCUSSION

In this study OSTR was extended to horizontal planar bilayers thus providing potentially access to a wide variety of transporters. A conservative count of candidate transporters which can be inserted into planar lipid bilayers and for which fluorescent substrates or substrate indicators are available such as translocases ($\sim$12 identified members; Agarraberes and Dice, 2001), ATP binding cassette (ABC) pumps ($\sim$50 identified members; Klein et al., 1999) and pore-forming toxins ($\sim$100 identified members; Gilbert, 2002) yields $\sim$100. If mutants created by recombinant methods for analytical, diagnostic, therapeutic, or biotechnological purposes are included quite large numbers arise. In addition, electrical and optical single transporter recording were partially amalgamated. In the following, the results of this study will be discussed in relation to the known properties of the α-HL pore, the possibilities offered by OSTR for the analysis of ''slow'' transporters such as translocases, and the potential impact of OSTR on the nanopore approach for the analysis of single molecules.

The α-HL protein (Bhakdi et al., 1996; Menestrina et al., 2003) is synthetized and released by *S. aureus* as a 293-residue water-soluble protein. Upon binding to cellular membranes the protein heptamerizes and a part of the oligomer inserts into the membrane. The crystal structure at 1.9 Å resolution of the detergent-solubilized α-HL pore (Song et al., 1996) shows a mushroomlike complex with a cap of $\sim$10 nm diameter and $\sim$7 nm length residing outside the membrane and a stem of $\sim$3 nm diameter and 5 nm length traversing the bilayer. The channel inside the α-HL pore starts at the cap with an entrance of 2.6 nm diameter, followed by a vestibule of 4.6 nm diameter, a limiting aperture of 1.5 nm diameter and a transmembrane part of 2.0 nm diameter. Electrical single channel recording (Krasilnikov et al., 1981; Menestrina, 1986; Korchev et al., 1995) showed that α-HL forms stable nongated pores in lipid bilayers with approximately ohmic characteristics, although some rectification and a mild anion selectivity were found. In 1M KCl a voltage difference of 120 mV yielded a current of 120 pA, consistent with these results (Fig. 2 *B* and Fig. 4, *B* and *C*). The functional diameter of the α-HL pore, determined in erythrocytes by osmotic protection experiments (Menestrina, 1986; Krasilnikov et al., 1988; Tejuca et al., 2001), was found to be 1.8–2.8 nm. Calcein and Ca^{2+} ions exhibit different hydrodynamic (Stokes) diameters of $\sim$0.65 nm and $\sim$0.29 nm, respectively, resulting in unitary permeabilities of 2.5×10^{-2} $\mu m^3 s^{-1}$ and 29×10^{-2} $\mu m^3 s^{-1}$. We previously observed a similar relationship for the slightly smaller aerolysin pore (Tschödrich-Rotter et al., 1996). The dependence of the unitary permeabilities on the hydrodynamic radius is a further clear hint to the dynamic range of ion permeabilities, which may be used by the biotechnological ''footprint'' approach analyzing the sequence of polynucleotides or peptides.

The translocation of newly synthetized proteins into the ER lumen as well as the insertion of transmembrane regions of membrane proteins into the ER membrane are mediated by a protein complex referred to as translocon (Walter and Lingappa, 1986; Rapoport et al., 1996; Johnson and van

Waes, 1999; Blobel, 1999). Electrical single channel recording (Simon et al., 1989), fluorescence spectroscopic studies (Crowley et al., 1994), cryoelectronmicroscopy (Beckmann et al., 1997; Menetret et al., 2000; Beckmann et al., 2001; Breyton et al., 2002), and x-ray diffraction (Van den Berg et al., 2004) all have indicated that translocation and insertion involves an aqueous transmembrane channel. Preliminary experiments (R. Hemmler, G. Böse, R. Wagner, and R. Peters, unpublished data) suggest that the experimental approach worked out in this study can be applied to measure the permeability of protein conducting channels for Calcein and Ca^{2+} ions. We therefore feel that it should become possible in the near future to directly measure also the translocation of proteins.

Support by the Volkswagen-Stiftung is gratefully acknowledged.

REFERENCES

Agarraberes, F. A., and J. F. Dice. 2001. Protein translocation across membranes. *Biochim. Biophys. Acta.* 1513:1–24.

Akeson, M., D. Branton, J. J. Kasianowicz, E. Brandin, and D. W. Deamer. 1999. Microsecond time-scale discrimination among polycytidylic acid, polyadenylic acid, and polyuridylic acid as homopolymers or as segments within single RNA molecules. *Biophys. J.* 77:3227–3233.

Bayley, H., and C. Cremer. 2001. Stochastic sensors inspired by biology. *Nature (Lond.).* 413:226–230.

Beckmann, R., D. Bubeck, R. Grassucci, P. Penczek, A. Verschoor, G. Blobel, and J. Frank. 1997. Alignment of conduits for the nascent polypeptide chain in the ribosome-Sec61 complex. *Science.* 278:2123–2126.

Beckmann, R., C. M. Spahn, N. Eswar, J. Helmers, P. A. Penczek, A. Sali, J. Frank, and G. Blobel. 2001. Architecture of the protein-conducting channel associated with the translating 80S ribosome. *Cell.* 107:361–372.

Bhakdi, S., H. Bayley, A. Valeva, I. Walev, B. Walker, U. Weller, M. Kehoe, and M. Palmer. 1996. Staphylococcal alpha-toxin, streptolysin-O, and *Escherichia coli* hemolysin: prototypes of pore-forming bacterial cytolysins. *Arch. Microbiol.* 165:73–79.

Blobel, G. 1999. Protein targeting. *Biosci. Rep.* 20:303–344.

Blobel, G., and B. Dobberstein. 1975. Transfer of proteins across membranes. I. Presence of proteolytically processed and unprocessed nascent immunoglobulin light chains on membrane-bound ribosomes of murine myeloma. *J. Cell Biol.* 67:835–851.

Breyton, C., W. Haase, T. A. Rapoport, W. Kuhlbrandt, and I. Collinson. 2002. Three-dimensional structure of the bacterial protein-translocation complex SecYEG. *Nature (Lond.).* 418:662–665.

Crowley, K. S., S. Liao, V. E. Worrell, G. D. Reinhart, and A. E. Johnson. 1994. Secretory proteins move through the endoplasmic reticulum membrane via an aqueous, gated pore. *Cell.* 78:461–471.

Favre, I., Y. M. Sun, and E. Moczydlowski. 2004. Reconstitution of native and cloned channels into planar bilayers. *Methods Enzymol.* 294:287–304.

Gilbert, R. J. C. 2002. Pore-forming toxins. *Cell. Mol. Life Sci.* 59:832–844.

Heins, L., A. Mehrle, R. Hemmler, R. Wagner, M. Küchler, F. Hörmann, D. Sveshnikov, and J. Soll. 2002. The preprotein conducting channel at the inner envelope membrane of plastids. *EMBO J.* 21:2616–2625.

Hill, K., K. Model, M. T. Ryan, K. Dietmeier, F. Martin, R. Wagner, and N. Pfanner. 1998. Tom40 forms the hydrophilic channel of the mitochondrial import pore for preproteins. *Nature (London).* 395:516–521.

Johnson, A. E., and M. A. van Waes. 1999. The translocon: a dynamic gateway at the ER membrane. *Annu. Rev. Cell Dev. Biol.* 15:799–842.

Kasianowicz, J. J., E. Brandin, D. Branton, and D. W. Deamer. 1996. Characterization of individual polynucleotide molecules using a membrane channel. *Proc. Natl. Acad. Sci. USA.* 93:13770–13773.

Kiskin, N., J. P. Siebrasse, and R. Peters. 2003. Optical microwell assay of membrane transport kinetics. *Biophys. J.* 85:2311–2322.

Klein, I., B. Sarkadi, and A. Varadi. 1999. An inventory of the human ABC proteins. *Biochim. Biophys. Acta.* 1461:237–262.

Korchev, Y. E., C. L. Bashford, G. M. Alder, J. J. Kasianowicz, and C. A. Pasternak. 1995. Low conductance states of a single ion channel are not 'closed'. *J. Membr. Biol.* 147:233–239.

Kovermann, P., K. N. Truscott, B. Guiard, P. Rehling, N. B. Sepuri, H. Müller, R. E. Jensen, R. Wagner, and N. Pfanner. 2002. Tim22, the essential core of the mitochondrial protein insertion complex, forms a voltage-activated and signal-gated channel. *Mol. Cell.* 9:363–373.

Krasilnikov, O. V., R. Z. Ssabirov, V. I. Ternovsky, P. G. Merzliak, and B. A. Tashmukhamedov. 1988. The structure of Staphylococcus aureus alpha-toxin-induced ionic channel. *J. Gen. Physiol.* 7:467–473.

Krasilnikov, O. V., V. I. Ternovsky, and B. A. Taschmukhamedov. 1981. Properties of conductivity channels induced in phospholipid bilayer membranes by alpha-staphylotoxin. *Biofizika.* 26:271–275.

Kubitscheck, U., O. Kückmann, T. Kues, and R. Peters. 2000. Imaging and tracking of single GFP molecules in solution. *Biophys. J.* 78:2170–2179.

Kubitscheck, U., and R. Peters. 1998. Localization of single nuclear pore complexes by confocal laser scanning microscopy and analysis of their distribution. *Methods Cell Biol.* 53:79–98.

Meller, A., L. Nivon, E. Brandin, J. Golovchenko, and D. Branton. 2000. Rapid nanopore discrimination between single polynucleotide molecules. *Proc. Natl. Acad. Sci. USA.* 97:1079–1084.

Menestrina, G. 1986. Ionic channels formed by Staphylococcus aureus alpha-toxin: voltage-dependent inhibition by divalent and trivalent cations. *J. Membr. Biol.* 90:177–190.

Menestrina, G., M. Dalla Sera, M. Comai, M. Coraiola, G. Viero, S. Werner, D. A. Colin, H. Monteil, and G. Prevost. 2003. Ion channels and bacterial infection: the case of beta-barrel pore-forming protein toxins of Staphylococcus aureus. *FEBS Lett.* 552:54–60.

Menetret, J. F., A. Neuhof, D. G. Morgan, K. Plath, M. Radermacher, T. A. Rapoport, and C. W. Akey. 2000. The structure of ribosome-channel complexes engaged in protein translocation. *Mol. Cell.* 6:1219–1232.

Micelli, S., E. Gallucci, D. Meleleo, V. Stipani, and V. Picciarelli. 2002. Mitochondrial porin incorporation into black lipid membranes: ionic and gating contribution to the total current. *Bioelectrochemistry.* 57:97–106.

Mueller, D., O. Rudin, H. T. Tien, and W. C. Wescott. 1962. Reconstruction of cell membrane structure in vitro and its transformation into an excitable system. *Nature (Lond.).* 194:979–980.

Peters, R. 2003. Optical single transporter recording: transport kinetics in microarrays of membrane patches. *Annu. Rev. Biophys. Biomol. Struct.* 32:47–67.

Peters, R., H. Sauer, J. Tschopp, and G. Fritzsch. 1990. Transients of perforin pore formation observed by fluorescence microscopic single channel recording. *EMBO J.* 9:2447–2451.

Rapoport, T. A., B. Jungnickel, and U. Kutay. 1996. Protein transport across the eukaryotic endoplasmic reticulum and bacterial inner membranes. *Annu. Rev. Biochem.* 65:271–303.

Rehling, P., K. Model, K. Brandner, P. Kovermann, A. Sickmann, H. E. Meyer, W. Kühlbrandt, R. Wagner, K. N. Truscott, and N. Pfanner. 2003. Protein insertion into the mitochondrial inner membrane by a twin-pore translocase. *Science.* 299:1747–1751.

Siebrasse, J. P., and R. Peters. 2002. Rapid translocation of NTF2 through the nuclear pore of isolated nuclei and nuclear envelopes. *EMBO Rep.* 3:887–892.

Simon, S. M., G. Blobel, and J. Zimmerberg. 1989. Large aqueous channels in membrane vesicles derived from the rough endoplasmic reticulum of

canine pancreas or the plasma membrane of *Escherichia coli*. *Proc. Natl. Acad. Sci. USA*. 86:6176–6180.

Song, L., M. R. Hobaugh, C. Shustak, S. Cheley, H. Bayley, and J. E. Gouaux. 1996. Structure of staphylococcal alpha-hemolysin, a heptameric transmembrane pore. *Science*. 274:1859–1866.

Tejuca, M., M. Dalla Sera, C. Alvarez, C. Potrich, and G. Menestrina. 2001. Sizing the radius of the pore formed in erythrocytes and lipid vesicles by the toxin sticholysin I from the sea anemone *Stichodactyla helianthus*. *J. Membr. Biol*. 183:125–135.

Truscott, K. N., P. Kovermann, A. Geissler, A. Merlin, M. Meijer, A. J. M. Driessen, J. Rassow, N. Pfanner, and R. Wagner. 2001. A presequence- and voltage-sensitive channel of the mitochondrial preprotein translocase formed by Tim23. *Nat. Struct. Biol*. 8:1074–1082.

Tschödrich-Rotter, M., U. Kubitscheck, G. Ugochukwu, J. T. Buckley, and R. Peters. 1996. Optical single-channel analysis of the aerolysin pore in erythrocyte membranes. *Biophys. J*. 70:723–732.

Tschödrich-Rotter, M., and R. Peters. 1998. An optical method for recording the activity of single transporters in membrane patches. *J. Microsc*. 192:114–125.

Van den Berg, B., W. M. Clemons, Jr., I. Collinson, Y. Modis, E. Hartmann, S. C. Harrison, and T. A. Rapoport. 2004. X-ray structure of a protein-conducting channel. *Nature (Lond.)*. 427:36–44.

Walter, P., and V. R. Lingappa. 1986. Mechanism of protein translocation across the endoplasmic reticulum membrane. *Annu. Rev. Cell Biol*. 2:499–516.